Energy & Buildings 323 (2024) 114794

Contents lists available at ScienceDirect

Energy & Buildings

journal homepage: www.elsevier.com/locate/enb

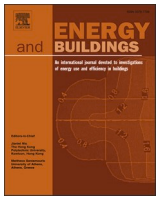

Experimental and computational assessment of an energy-saving innovation in a customised testing cabin

Grant Henshaw [a,1], Amin Deyranlou [b,c,1], Keith Rimmer [d], Heidi Paula Diaz Hernandez [a], Richard Fitton [a], Amir Keshmiri [c,*]

[a] Energy House Labs, University of Salford, Manchester M5 4WT, UK
[b] School of Engineering and Computing, University of Central Lancashire, PR1 2HE, UK
[c] School of Engineering, University of Manchester, M13 9PL, UK
[d] Thermocill Limited, Suite13, Peel House, 30 The Downs, Altrincham WA14 2PX, UK

ARTICLE INFO

Keywords:
Energy-saving
Heat transfer
Building
U-value
Experimental study
Computational Fluid Dynamics (CFD)

ABSTRACT

The aim of this paper is to assess the performance of an energy-saving device, called 'Thermocill' in a customised test cabin, located in a controlled environment. With the UK domestic energy sector responsible for nearly 27 % of the total energy mix in 2022, and massive increases in the cost of energy on homeowners and tenants, simple and low-cost retrofit measures could potentially be of great value, if they prove to be effective at saving energy. The paper describes the experimental and computational methods in detail with the goal of setting an important example/standard for the assessment of similar energy-saving innovations under the UK Standard Assessment Procedure (SAP). This, in turn, would enable the performance of such innovations to be captured in the Energy Performance Certificates (EPCs) for Building Regulation compliance. On that basis, a test cabin was constructed at Salford Energy house 2.0 to investigate Thermocill's impacts on energy consumption and loss within the cabin. The experimental procedure is subsequently compared against a series of Computational Fluid Dynamics (CFD) simulations conducted for a larger number of scenarios. The performance of Thermocill was explored at different room temperature setpoints (16, 21, and 24 °C), window types (air and argon-filled double-glazed), and with/without blinds. The results were presented for four main scenarios including 'cabin without Thermocill/blind', 'cabin with blind', 'cabin with Thermocill', and 'cabin with blind/Thermocill'. The results were presented in the form of U-values and heat losses for the windows, while additional results were provided from CFD simulations. A good correlation between the experiments and the CFD was found, showing confidence in both methods. Findings demonstrated that, when Thermocill is in operation, it reduces the average U-value by around 3–4 %, which is considered a significant payback for a passive and economical measure. The methodology presented in this paper is expected to set an important example/standard for the assessment of similar energy-saving innovations under UK SAP. This, in turn, would enable the performance of such innovations to be captured in the EPCs for Building Regulation compliance.

1. Introduction

Global warming is a worldwide challenge which threatens different regions across the earth. In response to this challenge, a worldwide initiative is underway to achieve net zero by 2050. The UK government put this target into law in 2021 while hosting the COP26 Summit [1], however, significant work and innovation are required to achieve this target.

The UK domestic sector was responsible for 26.9 % (34.3 Mtoe) of the total UK energy consumption in 2022, second only to transport [2]. Although this 34.3 Mtoe figure is a 14 % reduction from the previous year, this can be attributed to the fact that the 2022 UK average temperature achieved its highest recorded average, further highlighting the impact of climate change. In addition, the energy price cap increased significantly throughout 2022 (54 % in April, and a further 80 % in October), resulting in homeowners and tenants changing their energy

* Corresponding author.
E-mail address: a.keshmiri@manchester.ac.uk (A. Keshmiri).
[1] These authors contributed equally.

https://doi.org/10.1016/j.enbuild.2024.114794
Received 16 May 2024; Received in revised form 5 September 2024; Accepted 8 September 2024
Available online 12 September 2024

consumption behaviours [3].

To reduce the energy demand of the domestic sector, the UK Government has published their consultation of The Future Homes Standard [4], which requires newly built homes to be future-proofed with low carbon heating and world-leading levels of energy efficiency; it will be introduced by 2025. This new standard impacts all aspects of the home, including heating and energy systems, metering, and the building fabric. Although this is a welcome step to reduce the energy demand of the domestic sector in terms of new buildings, it does not address the more significant issue of retrofit. 70 % of the 2010 UK housing stock will still be in use in 2050 [5]. A key statistic of the UK policy paper "Net Zero Strategy: Build Back Better", states that 60 % of the UK's housing stock has an Energy Performance Certificate (EPC) rating of D or below [6]. It is clear that we need to reduce the energy consumption of the UK housing stock, and the major contributor is the poor fabric performance. Major retrofit interventions are costly, and most homeowners would require financial support to implement such retrofits, creating a need for innovative and low-cost solutions.

Many components of the building fabric can be improved with increased levels of insulation, so long as it is installed correctly [7]. However, one aspect which is more difficult to improve is the openings, in particular, the windows of a dwelling, which can account for 20–30 % of the total dwelling heat loss [8,9]. Although windows are a necessary part of the building fabric, they can be considered a "thermal hole", increasing the total heat transfer of a dwelling, and can also negatively impact occupant thermal comfort [10]. Although improvements can be made to the windows, such as increasing the performance of both the glazing and frame, as well as improving the airtightness, and applying coatings [11,12] these are typically costly, difficult and invasive interventions. Other strategies to reduce heat transfer through windows are the use of window coverings and the installation of radiators close to windows [13–18]. Furthermore, Fitton et al. [19] and Henshaw et al. [20] have characterised the in-situ thermal performance of window coverings under controlled conditions. This was achieved by quantifying the reduction in the window U-value through a relatively simple experimental design, adapted from that which is described in ISO 9869-1 [21]. However, most of these strategies do not heat, but instead cover the cold surface produced by the window. If warm air can bypass such covering, which is often the case, heat transfer will still occur resulting from the cold surface of the window. Moreover, in cases with a relatively large surface-to-air temperature difference, this can result in a condensation risk [22].

The present work studies a new innovation in the building energy sector, called *Thermocill*^{TM}. Thermocill is an energy-saving product, developed by Thermocill Limited, that is designed for installation under the window board and above the radiator in a room, which is made from recycled Nylon materials and can be retrofitted to existing homes as well as new builds. In its operation, the product tends to direct the natural convection from the radiator to create a wall of warm air immediately in front of the glazing on the internal side. The size and thickness of the warm air depend on many factors including radiator capacity, room set temperature, the distance between the radiator and Thermocill, the temperature in the room, the overhang of the Thermocill over a radiator, and the size/shape of the window sill/window reveal. It aims to prevent heat loss through increasing the surface temperature, and stop cold air from entering the room, in a similar manner to an "air curtain". Thermocill units has a modular and telescopic nature and comes in individual units (discussed further in Section 2.1.1, below). The size of Thermocill is only determined by the available space in the window sill and can be installed in a wide range of window reveals. It is relatively low-cost and simple to install building components, making it viable for both new builds and retrofit.

Keshmiri [23] studied the effects of Thermocill on condensation and moisture around the windows (the discussion of which is beyond the scope of the present work) and further conducted energy modelling for a typical UK house in order to calculate the potential energy and CO2 emission savings as a result of installing Thermocill in the bedrooms and the living room. Building upon the findings and limitations of the work presented in Keshmiri [23], the present research aims to quantify the in-situ thermal performance of Thermocill under controlled conditions, assessing if the product reduces heat transfer through the glazing panel of a window under a range of environmental conditions. The results of this experimental work will be used to calibrate a Computational Fluid Dynamics (CFD) model, which will then be used to assess the thermal performance of Thermocill under a wider range of environmental conditions. In addition, the proposed framework and its outcome in this project would enable Thermocill to complete the 'New Technology Process' as part of the Standard Assessment Procedure (SAP). SAP is managed through the Building Research Establishment (BRE) on behalf of the UK Government and is used for EPCs and Building Regulation compliance. The testing procedure outlined in this paper can easily be adapted and applied to other new/innovative technologies associated with building energy.

2. Methodology

2.1. Experimental research facility

Salford Energy House 2.0 is a globally unique research facility focusing on Building Performance Evaluation (BPE). Based at the University of Salford, the facility consists of two independent environmental chambers, capable of replicating 95 % of the populated world through both steady-state and dynamic control of temperature (−20 °C to + 40 °C), humidity, wind, rain, snow and solar gains. Each chamber is capable of housing two full-scale detached dwellings, which can be constructed, tested, and demolished. The Thermocill testing took place in a bespoke test cabin, located in Chamber 2. Fig. 1 shows two scenes from the Energy House 2.0.

2.1.1. Test cabin and Thermocill

The bespoke cabin was designed to have two separate Double-Glazed Units (DGU), one air-filled, and another argon-filled, with the latter having a greater thermal performance. The walls surrounding the DGUs were retrofitted to be of a similar thermal performance to a typical UK wall.

Each DGU has a RadiWarm Signature HE4140 electrically powered wet radiator system [24] located beneath, with a variable 1.625 kW power output. Each radiator is independently controlled by the RadiWarm 7-day programmable controller, which was located on a tripod at mid-room height at the centre of the rear cabin wall. Fig. 2 shows the cabin during different preparation stages.

The detailed dimensions of the cabin, blind, and Thermocill are demonstrated in Figs. 3 and 4.

Both DGUs have a standard roller-blind fitted, which can be easily unclipped from their brackets for different test scenarios. When the blinds are "closed", it is assumed that they stand 1 mm above the windowsill surface and have a 0.5 mm gap from either side of the wall (Fig. 3-c). Thermocill as explained earlier in the introduction, is an innovative passive window board that redirects the warm air from the radiators below the windows up and close to the glazing. As a result, it can create a thermal boundary that potentially reduces energy loss from the windows, and condensation on the windows. Thermocill has a simple and effective design. As shown in Fig. 4, it has an opening with a height of 16 mm, a vent length of 9 mm, an overhang length of 75 mm, and a lip height of 26 mm.

2.2. Experimental procedure

2.2.1. Design

The experimental test conditions are shown in Table 1. Due to time constraints, the experimental work only considered the air-filled DGU, and three different environmental conditions, all deemed "typical" of

Fig. 1. (a) Front elevation, (b) Chamber 1 with experimental homes.

Fig. 2. The Thermocill testing cabin at Salford Energy House 2.0, housed at the University of Salford.

those which would be found in an occupied property within the UK during the winter heating season [25].

The heat flux through the centre of the air-filled DGU was measured using Hukseflux HFP-01 heat flux plates (HFP). The HFP were affixed to the internal surface of the DGU using thermal contact paste and adhesive tape, as shown in Fig. 5. The ΔT for each in-situ U-value measurement was calculated using the internal and external air temperature differential measured at the geometric centre of the cabin and within the climatic chamber. For U-values calculations, measurements were taken every minute, however, these were aggregated into 10-minute averages for the analysis.

2.2.2. *In-situ U-value and its uncertainty*

The thermal transmittance of a building element (U-value) is defined

No	Part
1	Radiator
2	Argon-filled Double-glazed + blind
3	Air-filled double-glazed + blind
4	Door
5	Front window (single glazed)
6	Thermocill
7	Vent

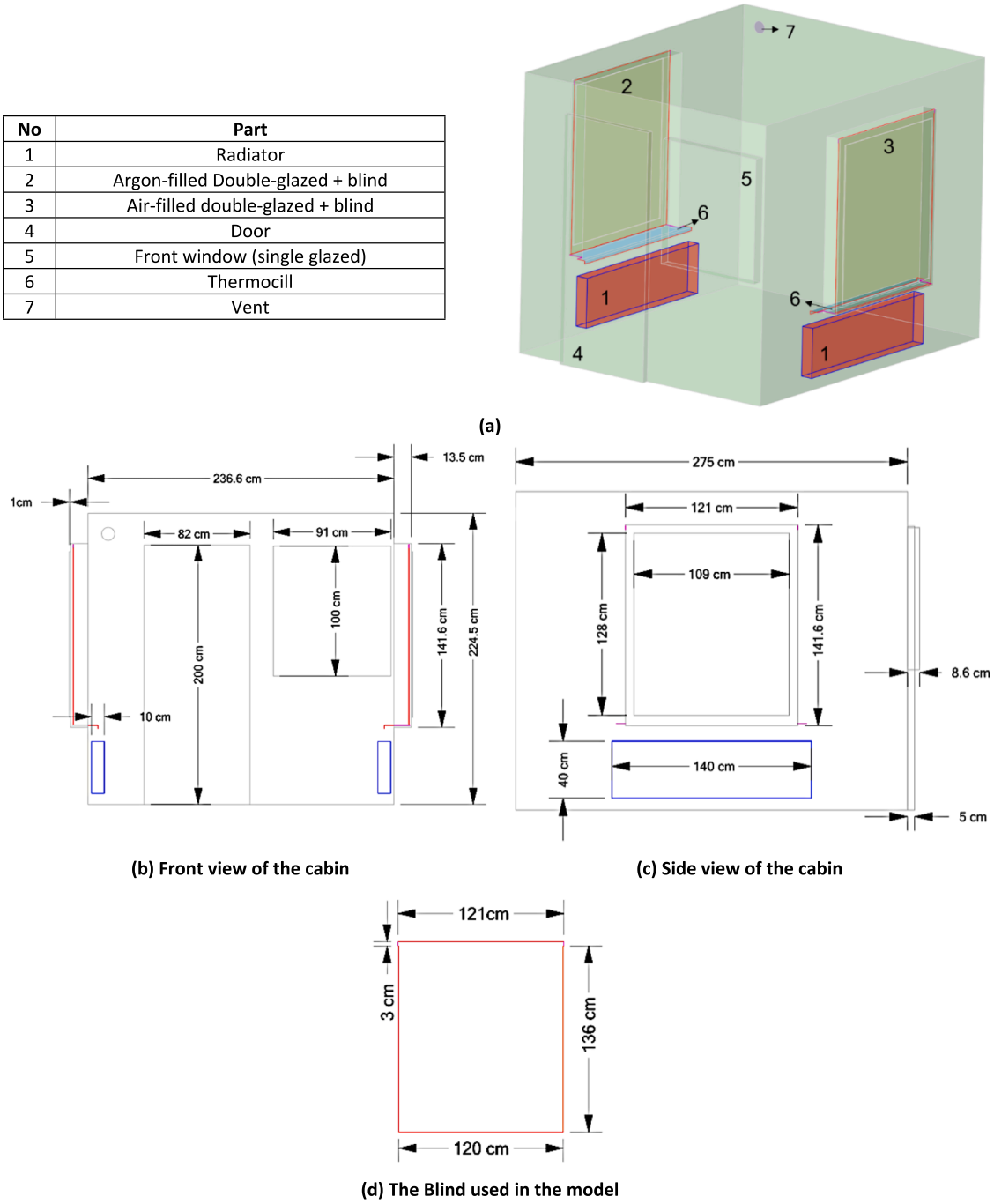

Fig. 3. (a) An employed CAD model for the computer simulation with details of different parts, (b–d) Dimensions of the test cabin and the main components,

in ISO 7345 as the *"Heat flow rate in the steady state divided by area and by the temperature difference between the surroundings on each side of a system"*. ISO 9869-1 uses a cumulative moving average of the heat flow rate and ΔT to calculate in-situ U-values of opaque building elements, to account for thermal storage and release. However, steady-state conditions within Energy House 2.0, and the lack of solar radiation, allow the U-value to be calculated by an amalgamation of ISO 7345 [26] and ISO 9869-1 [21] using the following equation:

$$U = \frac{q}{\Delta T} \tag{1}$$

where U is the U-value [W/m^{2}K], q denotes the heat flux [W/m^2] across the windows, and ΔT [K] is the air temperature difference. A similar formula was used to estimate U-values in the CFD simulations in which steady-state heat transfer is assumed. Noteworthy to mention that in obtaining steady-state energy flow, the CFD approach is different from the experiment. These values are estimated by assuming no temporal variations in the conservation of mass, momentum, and energy equations.

2.2.3. *In-situ U-value uncertainty under controlled conditions*

The testing conducted within the Thermocill cabin at Energy House 2.0 allowed for both stable and undisturbed testing. An uncertainty methodology was produced following the GUM method [27].

Type A uncertainty

The Type A uncertainty considers the statistical variation in the measured data. For U-value calculations, data was aggregated into 10 min averages. The uncertainty of this data has been calculated as the

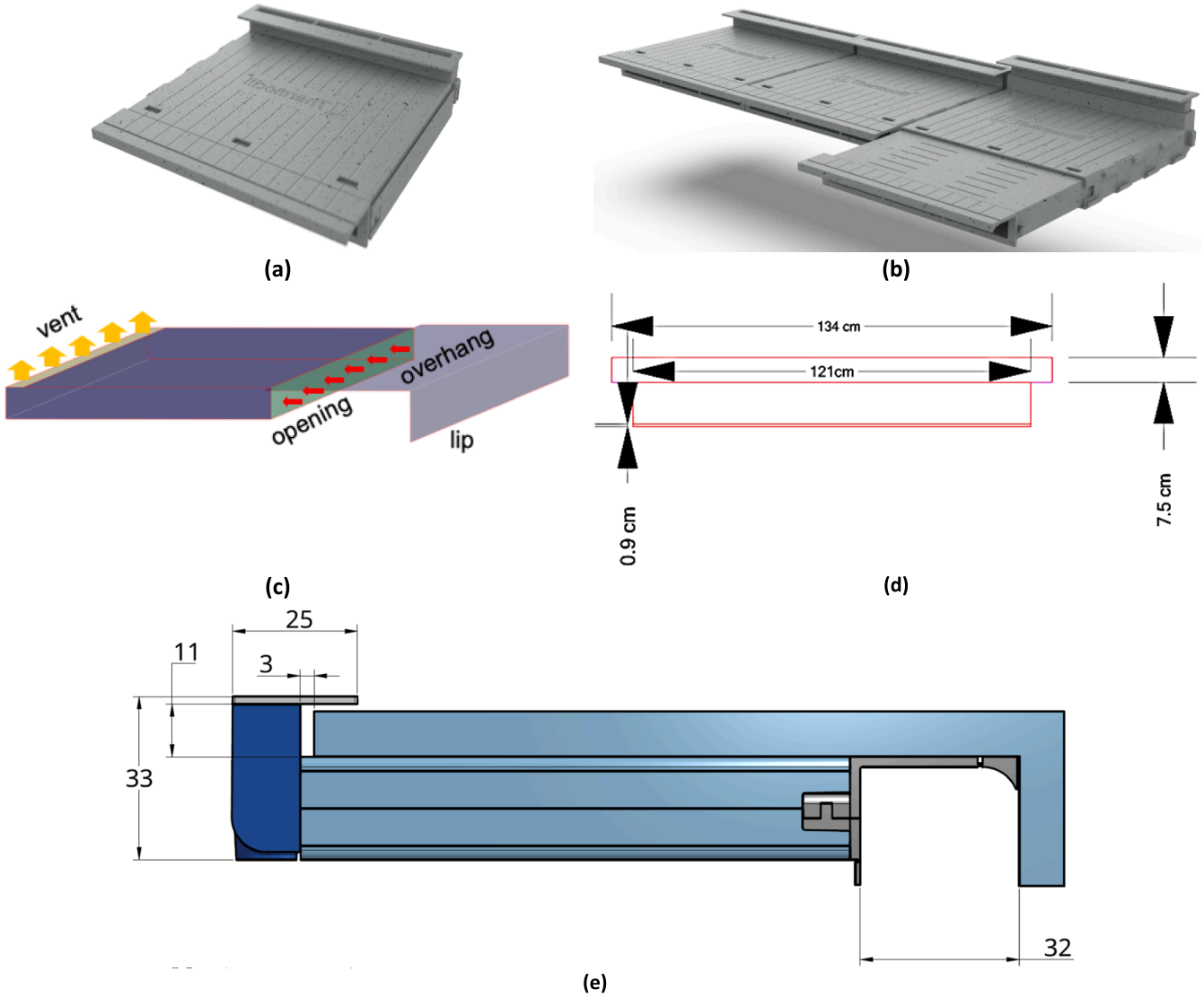

Fig. 4. Schematics of (a) a single Thermocill unit, (b) assembly of 3 Thermocill units, (c) a simplified Thermocill unit implemented in the CFD simulations. Dimensions of (d) the front view of the Thermocill assembly implemented in the CFD simulations (lip: 2.6 cm, overhang: 7.5 cm, opening: 1.6 cm, and vent: 0.9 cm) and (e) the side view of the original Thermocill unit (in mm).

Table 1
Experimental test conditions.

Test	Reference*	Internal temperature [°C]	External temperature [°C]	Glazing type	Window covering	Thermocill installed
1a	C(21)	21.0	4.7	Air-filled	NO	NO
1b	CT(21)	21.0	4.7	Air-filled	NO	YES
2a	CB(21)	21.0	4.7	Air-filled	YES	NO
2b	CBT(21)	21.0	4.7	Air-filled	YES	YES
3a	C(24)	24.0	4.7	Air-filled	NO	NO
3b	CT(24)	24.0	4.7	Air-filled	NO	YES

*C = Cabin; T = Thermocill; B = Blind.

standard error of these averages.

$$u_A = \frac{\sigma}{\sqrt{n}} \tag{2}$$

where u_A is Type A uncertainty; σ is the standard deviation; and n defines the number of measurements.

Type B uncertainty

Table 2 details the Type B uncertainties associated with the equipment used.

Combined uncertainty

Type A and Type B uncertainties associated with a measurement are combined as follows:

$$u_{Combined} = \sqrt{u_A^2 + u_B^2} \tag{3}$$

where u_A and u_B are type A and B uncertainties, respectively.

Uncertainty propagation

The above uncertainty was calculated for the centre-pane heat flux

Fig. 5. Experimental equipment setup in the cabin.

Table 2
Measurement equipment used in the Energy House Thermocill performance tests.

Measurement	Equipment	Uncertainty[1]
Room air temperatures	hygroVUE 10 (20–60 °C)[2]	±0.1 °C
Chamber air temperatures	hygroVUE 10 (–40 to 70 °C)[2]	±0.2 °C
Internal air temperatures	Type-T thermocouple[3]	±0.1 °C
Heat flux	Hukseflux HFP-01 heat flux plate[4]	±6%

[1] Uncertainties were taken from supplier data sheet.
[2] HygroVUE10 – Digital Temperature and Relative Humidity Sensor with M12 Connector [34].
[3] Energy House 2.0 in house calibration process.
[4] HFP01 heat flux plate | Hukseflux | the world's most popular heat flux sensor [35].

and for both the internal and external air temperatures. Taking Eq. (3), uncertainty propagation yields the following equation:

$$u_{U-value} = \sqrt{\left(\frac{u_q}{\Delta T}\right)^2 + \left(\frac{q^2}{\Delta T^4}\right)\cdot\left(u_{T_i}^2 + u_{T_e}^2\right)} \tag{4}$$

where u_q [W m^{-2}] is the heat flux uncertainty, ΔT [K] denotes the temperature difference between the inside and outside of the cabin; q [Wm^{-2}] is the heat flux, and u_{T_i} [°C] and u_{T_e} [°C] represent internal and external temperature uncertainties, respectively.

Expanded uncertainty

Furthermore, when stating the uncertainty, the expanded uncertainty ($k = 1.96$) is given, such that:

$$U_{expanded} = k{\cdot}u \tag{5}$$

where $U_{expanded}$ is the expanded uncertainty; k is the coverage factor, and u is the uncertainty yielded through propagation. Such a coverage factor results in a 95 % confidence interval. This expanded uncertainty is used throughout the experimental results of this paper.

2.2.4. Experimental setup

13 Hukseflux HFP01 heat flux plates (HFPs) were set up across the DGU. This study will consider the centre pane U-value and also produce plots showing U-value reduction from the 13 HFPs measured across the DGU. Both internal and external air temperature measurements were taken using Hygrovue10 sensors [34]. Type-T thermocouples were used for local air and surface temperature measurements. A schematic diagram of the sensors used is shown in Fig. 6.

To reduce the uncertainty associated with the measurement, great care was taken to achieve a stable internal environment. Accordingly, the power output of the radiators was finely tuned to reduce the levels of hysteresis, which took significantly longer than expected.

It is worth noting that the cabin is tested under fully controlled environmental conditions, which would naturally lead to accurate and faster measurements compared to what can be achieved in fieldwork. However, as a result, some natural conditions such as solar gain/radiation and wind and other external flow conditions cannot be accounted for. While these are important factors in terms of heating and energy of a house, since the impact of Thermocill is mainly through convection inside the building, such external effects are not expected to have any significant impact on the effectiveness or performance of Thermocill.

2.3. CFD model

2.3.1. CFD overview

CFD is a powerful tool that can complement experiments and is a reliable alternative to exploring different physical phenomena using computer simulation. The present authors have previously applied CFD simulations to similar problems related to environmental flows and/or buildings with a good level of accuracy and success [28–30]. In this paper, CFD is selected for assessing Thermocill performance in different cabin conditions. Generally, the CFD pipeline comprises four stages including generating the physical domain (geometry), creating a high-resolution grid network (mesh), setting up the physical model through the governing equations (conservation of mass, momentum, and energy), appropriate boundary conditions, and numerical methods, and finally running the simulation and post-processing the results. In subsequent sections, each stage will be explained in detail.

2.3.2. The cabin geometry and mesh

The base CAD model of the cabin was provided to the University of Manchester by the research team at Energy House Labs. Subsequently, to prepare CFD-ready geometries (the cabin, radiators, Thermocill and blinds), several rounds of modifications were made to the CAD model to prepare it for the CFD simulation. Finally, four different CAD models were created including (i) cabin without blind/Thermocill, (ii) cabin with blinds only, (iii) cabin with Thermocill only, (iv) cabin with blinds/Thermocill. Fig. 3(a) shows an example of one of the final models, which

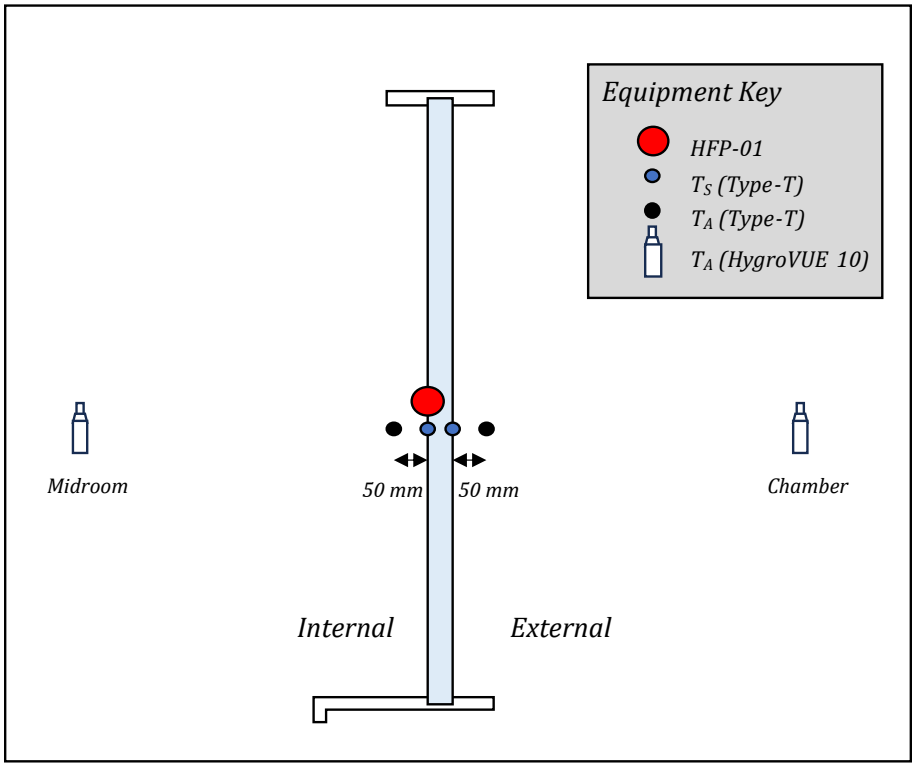

Fig. 6. Schematic diagram of sensors used for the analysis within this report.

is a cabin with two blinds and Thermocill units.

When a room is heated with radiators up to certain temperature setpoints, the air in the vicinity of the radiator warms up and starts rising due to natural convection, and gradually distributes the heat to the entire room. To capture all flow movements, the velocity and pressure distributions need to be precisely calculated, which are then employed in the energy equations to obtain temperature distribution and heat transfer to the outside [31,32]. Therefore, high-resolution meshes are required to sufficiently split the computational domain into small elements, which can detect all important features of flow and temperature,

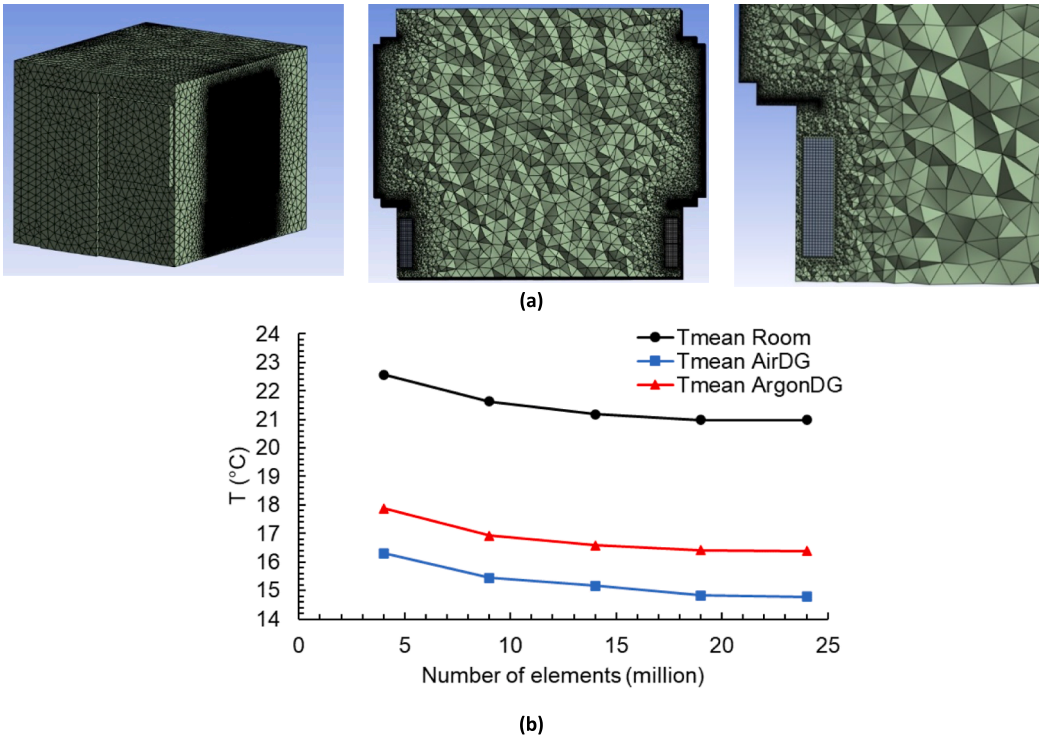

Fig. 7. (a) An example of the generated mesh for the case of the cabin with Thermocill, (b) mesh independency test for the mean temperature of the room, mean surface temperature of Air-filled Double Glazing (DG) and Argon-filled DG.

specifically for the regions where these variables experience high gradients. Several rounds of mesh independence study were conducted before choosing the final mesh. Finally, 8.9, 11.8, 16.1, and 19 million mesh sizes were selected for the cabin, cabin & Thermocill, cabin & blind, and cabin & blind & Thermocill cases, respectively. The finest mesh belongs to the case in which blind and Thermocill are in operation to capture flow and heat distributions accurately in the vicinity of these regions.

Fig. 7 illustrates an example meshed domain for the case of the cabin with Thermocill. In all the models, to maintain accuracy and keep the computational costs low, mesh is highly refined adjacent to the radiators, blinds, and Thermocill.

2.3.3. Assumptions and modelling choices

Different sets of equations were employed to model and simulate the heat transfer inside the cabin. Equations for the conservation of mass and momentum of the flow (Navier-Stokes equations), heat transfer equation (energy equation), and radiation equation were invoked to resolve flow and temperature distribution inside the cabin and heat transfer between the cabin and the outside environment.

In the natural convection phenomenon, gravitational acceleration, which is assumed to be 9.81 m/s^2 is the main player in inducing movement to the heated air. Therefore, given the air plume velocity and Rayleigh number, the Shear Stress Transport (SST) $\boldsymbol{k}$–ω turbulence model [33] is deemed to be a reasonable selection. Furthermore, since the air density does not change significantly within the considered temperature range inside the cabin, the Boussinesq approximation is employed in the model. Finally, the radiation inside the cabin was considered, to account for any radiative heat transfer from the radiators, albeit, they are not considered to be significant in this case. To account for air contribution in radiation, the Discrete Ordinates (DO) method was employed, which can consider the surface-to-surface and air radiations. The standard air property was chosen with the density set as 1.225 kg/m^3, the dynamic viscosity as 1.79×10^{-5} kg/m.s, the specific heat and thermal conductivity set as 1006.4 J/kg.K and 2.42×10^{-2} W/m.K, respectively. Finally, the air thermal expansion coefficient is assumed to be 3.4×10^{-3} 1/K.

One of the critical stages of the modelling is the selection of appropriate boundary conditions for different types of surfaces at boundaries and inside the cabin. For the momentum equations, the no-slip condition (zero velocity on the surface) was considered. Also, for the thermal boundary condition, appropriate U-values (provided by Salford Energy House 2.0) were adopted, as shown in Table 3.

It is worth mentioning that for all the test cases, the outside temperature is assumed to be 5 °C. Moreover, for the internal surfaces, which have interfaces with air (i.e., radiators, blinds, and Thermocill), heat flux continuity is considered to couple surfaces with the fluid domain (air). Finally, for the radiation equation, all the surfaces are considered to be opaque and diffuse surface (without specular reflection) with an internal emissivity of 0.9.

In the models, the radiators are considered as solid heat sources that have interfaces with air inside the room. In order to maintain the setpoint temperatures inside the room (i.e., 16 °C, 21 °C, 24 °C), the total heat loss from the cabin for each setpoint is imposed as the total required heat that should be provided by the heaters.

Generally, for natural convection problems, reaching equilibrium requires a larger number of timesteps and iterations. Therefore, choosing appropriate initial values and using a quasi-steady approach reduce the simulation time significantly. Therefore, this study benefitted from quasi-steady simulation and considering the initial temperature as such, which is equal to the setpoint temperature. Finally, to solve the governing equations numerically, ANSYS-FLUENT (2023R1) was employed.

Table 3
U-values for different sections of the cabin exposed to the surrounding.

No.	Surface	U-value (W/m^2K)
1	Ceiling	0.48
2	Floor	1.20
3	Front & Back Walls	0.70
4	Left and Right Walls	0.83
5	Air-filled double glazing	2.40
6	Argon-filled double glazing	1.30
7	Single glazing window	2.66
8	Door	2.54

3. Results

3.1. Experimental results and discussion

Thermocill was tested under controlled conditions at the Energy House 2.0 research facility, in which the external air temperature maintained a constant 5.2 °C (±0.1 °C) throughout all tests.

3.1.1. Centre pane U-value

Fig. 8 and Table 4 show the centre pane experimental results of all test scenarios. In both 21 °C internal condition scenarios (Tests 1 and 2), a reduction in the centre pane U-value of 4 % and 2 % respectively, was attributed to Thermocill. However, in Test 3, Thermocill showed an increase in centre pane U-value, when internal conditions were increased to 24 °C.

3.1.2. U-value distribution across glazing panel

The U-value percentage reduction was calculated for each heat flux plate measurement location. The below plots show how the U-value reduction varied spatially across the glazing panel, with blue indicating reductions in U-value, and red showing an increase in the U-value.

The mid-room internal temperature sensors and the chamber temperature sensor were used to calculate the U-values, in the same manner as the centre pane U-value.

Fig. 9 shows a greater reduction in U-value towards the bottom of the DGU (i.e., closer to the vents of the Thermocill product). As the height increases, the U-value reduction tends to reduce. In the case of "C(24) *vs* CT(24)", an increase in the measured U-value can be seen above the mid-height of the DGU.

Fig. 9 shows that Thermocill produced greater reductions in the measured U-value towards the bottom of the windowpane, i.e., closer to the vents of the Thermocill product. The reduction in the U-value tends to reduce as the height from the Thermocill product increases. In Test 3 (24 °C), the U-value increases beyond the middle height of the window. Table 5 shows the reduction and associated uncertainty for each HFP location and the average across all HFPs.

3.2. CFD results and discussion

In this section, the CFD results of the simulated cabin are presented. The results show flow and temperature distribution for the four aforementioned scenarios, and three setpoint temperatures (16, 21, and 24 °C). For the qualitative results, including streamlines in the vicinity of the radiators, volume-rendered temperature inside the cabin, and heat flux across air/argon-filled DGU the focus is on the setpoint temperature of 21 °C.

3.2.1. Qualitative results

Starting with the velocity streamline in Fig. 10, the results show that when a Thermocill is in operation it slightly deflects the hot plume near the radiators, therefore, the air rise velocity next to the windows is less than the cases without a Thermocill, however, it is more uniform and widened near the windows. Fig. 11 demonstrates volume-rendered temperature contours, which are capped between 21.5 °C and 23 °C for the setpoint of 21 °C. One point to emerge from the temperature contours is that in the presence of Thermocill, the temperature

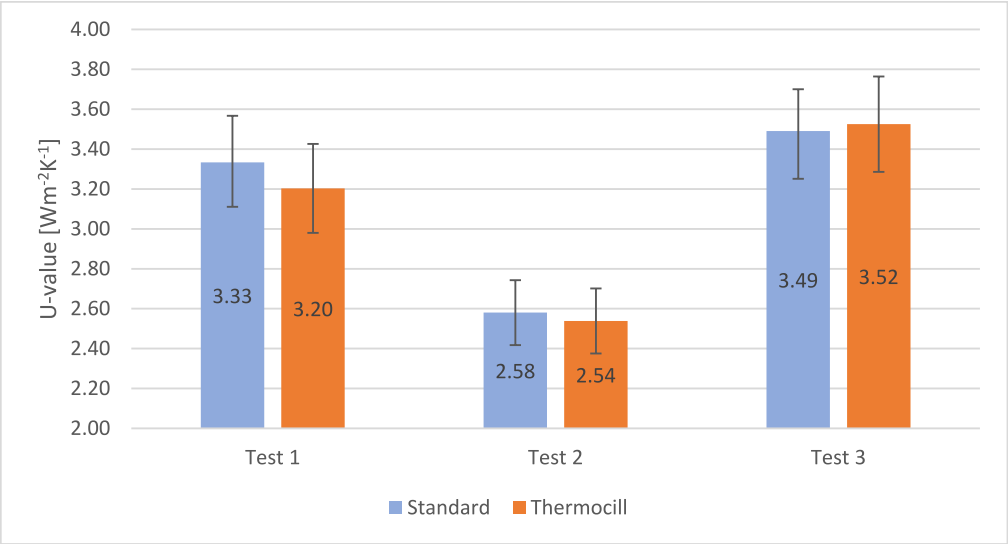

Fig. 8. Comparing the U-values in three performed experiments.

Table 4
Comparison of all experimental tests and relative reduction in centre pane U-Value.

Test	Reference	U-Value (W/m^{2}K)	Δ U-Value (W/m^{2}K)	% Reduction
1a (Standard)	C(21)	3.33 (±0.23)		
1b (Thermocill)	CT(21)	3.20 (±0.22)	−0.13 (±0.32)	4 % (±10 %)
2a (Standard)	CB(21)	2.58 (±0.16)		
2b (Thermocill)	CBT(21)	2.54 (±0.16)	−0.04 (±0.23)	2 % (±9%)
3a (Standard)	C(24)	3.49 (±0.21)		
3b (Thermocill)	CT(24)	3.52 (±0.24)	0.03 (±0.32)	−1% (±9%)

C: Cabin, T: Thermocill, B: Blind.

distribution is slightly more uniform next to the windows as the hot spot area is smaller compared to the cases in which the Thermocill is not operating. If the latter finding links to the heat loss results presented in Table 6, it shows that Thermocill tends to reduce heat loss through the windows both by creating a thermal layer next to the windows and directing a portion of the warmer air to the centre of the cabin.

Figs. 12 and 13 demonstrate heat flux from air-filled and argon-filled double-glazed windows, respectively. The results show that Thermocill can deviate the heat flux from the centre of the windows to the sides and reduce heat loss. Additionally, the blind acts as a thermal barrier, and therefore, as expected, when it is in operation, it significantly reduces the heat loss through the windows, as well as providing a more uniform heat flux distribution on the glazing. Considering the combined impact of the Thermocill and the blind, it is evident that the impact is aggregated and results in further reduction of heat loss through the windows.

3.2.2. *Quantitative results*

Further investigation was carried out to assess the impact of blind and Thermocill on the reduction of the heat loss from the cabin by comparing four different scenarios. Irrespective of the cabin temperature, simultaneous operation of the blind and Thermocill reduces the heat loss by at least 2 %. Furthermore, to explore the standalone impact of Thermocill, the results show that when it is used without any blind, it can save heat by 1 %, which shows a significant improvement given Thermocill's installation time and cost. Table 6 demonstrates the percentage of the total heat loss reduction inside the cabin by comparing four scenarios. Irrespective of the cabin temperature, simultaneous operation of the blind and Thermocill reduces the heat loss by at least 2 %.

One approach to specifically measure the impact of blinds and Thermocill on thermal efficiency is comparing the U-value for different scenarios. The cabin contains two double-glazed windows, one filled with air and another with argon. In this section, the room U-values for each double-glazed window are reported based on Eq. (1).

In Eq. (1), the mean internal surface temperature is calculated for the corresponding window for which the U-value is estimated. Furthermore, the outside temperature is assumed constant and equal to 5 °C for all cases. Table 7 displays U-values for the air double-glazed window in four simulated scenarios. It highlights that the blind and Thermocill move in favour of better insulation, i.e., they both reduce U-values as such for all the setpoints, the simultaneous operation of blind and Thermocill results in the lowest U-values. Specifically, about Thermocill performance, Table 8 compares the performance of Thermocill in cases with and without blind. The results show that Thermocill potentially reduces room U-values based on air double-glazed from a minimum of 2 % up to around 4.4 %. Also, when it is in operation with a blind, it improves the U-value by 4.1 %.

Similar results are obtained for the argon-filled double-glazed window in Tables 9 and 10. Generally, U-values are the minimum in all setpoints, when blind and Thermocill are used together. Additionally, there is a consistent pattern for that window, where, as the temperature setpoint increases, the efficiency of the blind and Thermocill reduces, while they still improve room U-values.

Fig. 14 summarises the Thermocill performance and its impacts on room U-value. In this figure, the focus is on the impact of Thermocill and hence in all comparisons, inclusion/exclusion of Thermocill is the main difference to enable the assessment of its performance in isolation i.e., '*cabin*' versus '*cabin and Thermocill*', and '*cabin and blind*' versus '*cabin, blind, and Thermocill*'. The results show that although we cannot follow a consistent pattern, the presence of Thermocill reduces the U-values by 1–5 % for the explored cases.

Fig. 9. Reference of heat flux plate number and corresponding location, plus spatial U-value reduction for each test.

Table 5
U-Value reduction for each Heat Flux Plates across all tests.

	Test		
	C(21) *vs* CT(21)	**CB(21) *vs* CBT(21)**	**C(24) *vs* CT(24)**
HFP 1	7 % (±9%)	−5% (±9%)	19 % (±8%)
HFP 2	3 % (±9%)	6 % (±9%)	11 % (±8%)
HFP 3	12 % (±9%)	11 % (±9%)	8 % (±8%)
HFP 4	1 % (±10 %)	10 % (±9%)	3 % (±9%)
HFP 5	2 % (±9%)	7 % (±8%)	−1% (±9%)
HFP 6	12 % (±9%)	9 % (±8%)	11 % (±9%)
HFP 7	−1% (±10 %)	4 % (±9%)	−2% (±9%)
HFP 8	0 % (±10 %)	3 % (±9%)	−4% (±9%)
HFP 9	4 % (±10 %)	2 % (±9%)	−1% (±9%)
HFP 10	−1% (±10 %)	0 % (±9%)	1 % (±9%)
HFP 11	−6% (±10 %)	6 % (±9%)	−4% (±9%)
HFP 12	4 % (±9%)	0 % (±8%)	−3% (±9%)
HFP 13	0 % (±10 %)	0 % (±9%)	−2% (±9%)
Average	**3 % (±5%)**	**4 % (±5%)**	**3 % (±7%)**

3.2.3. *U-value and energy saving*

In terms of building energy performance, it is desirable to develop a direct relationship between the U-value reduction of glazing units to the energy savings of a building. Keshmiri [23] conducted a series of building energy modelling for a 3-bedroom semi-detached house (a typical dwelling in the UK) in order to calculate the potential energy and CO_2 emission savings as a result of installing Thermocill in the bedrooms and the living room. This study provided valuable insight into the relationship between U-values of windows and energy/CO_2 emission savings in the specific house/scenarios in the work. The limitation of that study, however, was that the U-value reduction of the glazing by installing the Thermocill was taken as a fixed value, obtained from an earlier experimental study conducted at Salford Energy House. This limitation in fact was of the motivation behind the present study. Nevertheless, energy modelling for different buildings needs to be carried out to establish the link between U-values in glazing and energy consumption/saving in the building.

3.3. *Comparison/validation of CFD vs experiment*

Experimentally, Thermocill was shown to reduce the average U-value of the air-filled DGU by 3–4 % in all tests conducted. When considering the CFD simulations, Thermocill was shown to reduce the glazing panels' U-value by 2–4 % in all tests. The validity of the results is strengthened when considering the good level of agreement between the experimental and CFD work, which is highlighted in Table 11 and Fig. 15.

4. Limitations and future directions

Like any other study, there are limitations in the present work that are worth highlighting:

- The CFD models considered the Thermocill operation in a fully controlled room condition. Therefore, variations in outside temperature and radiator performance are not considered in the model. The air tightness data of the cabin was also not considered, as this information was not available at the time of running the simulations.
- In the CFD model, the size and operation of the blinds in the simulations are fixed. The exact gaps around the blinds were not available

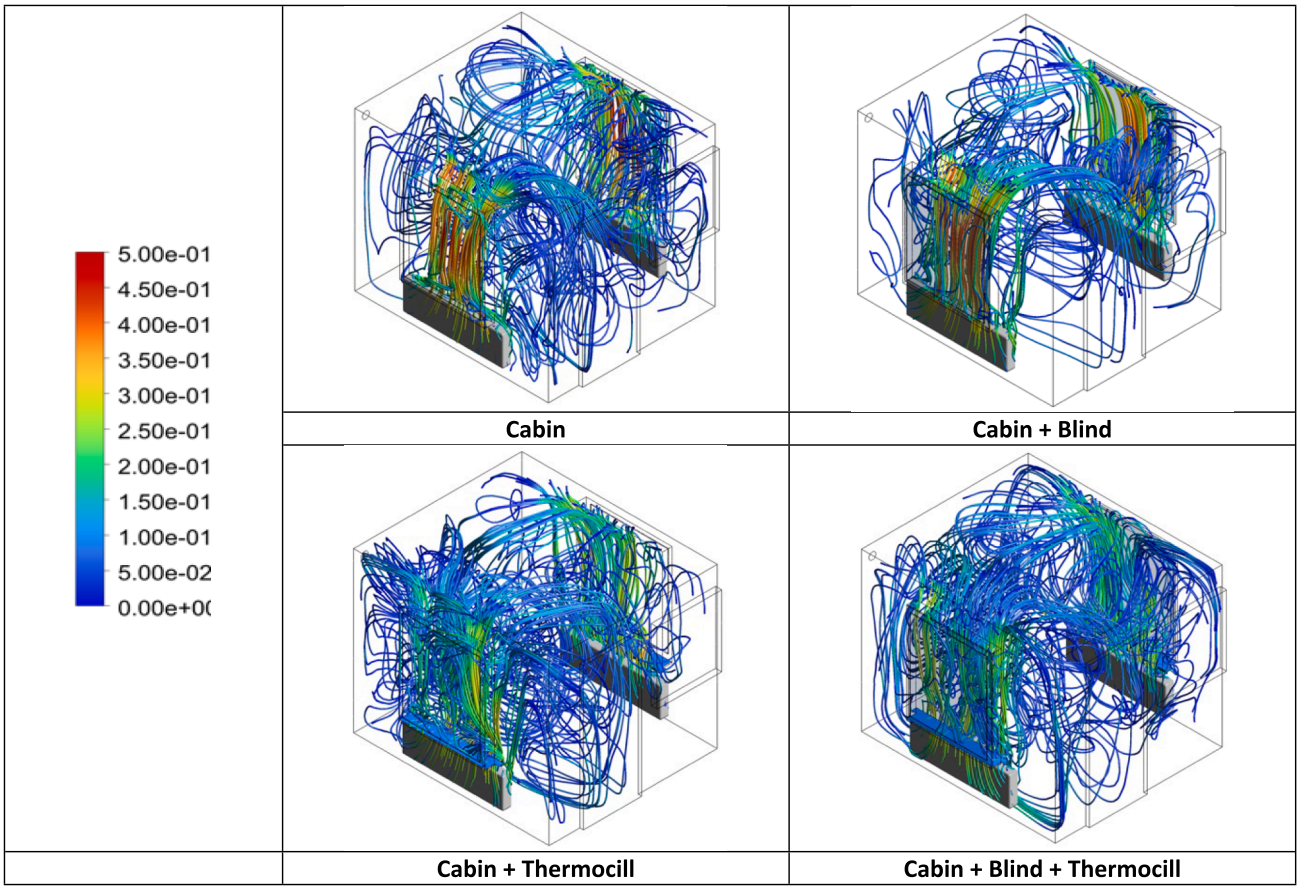

Fig. 10. Velocity streamlines (m/s) (starting from the radiators) for different test cases and the setpoint of 21 °C.

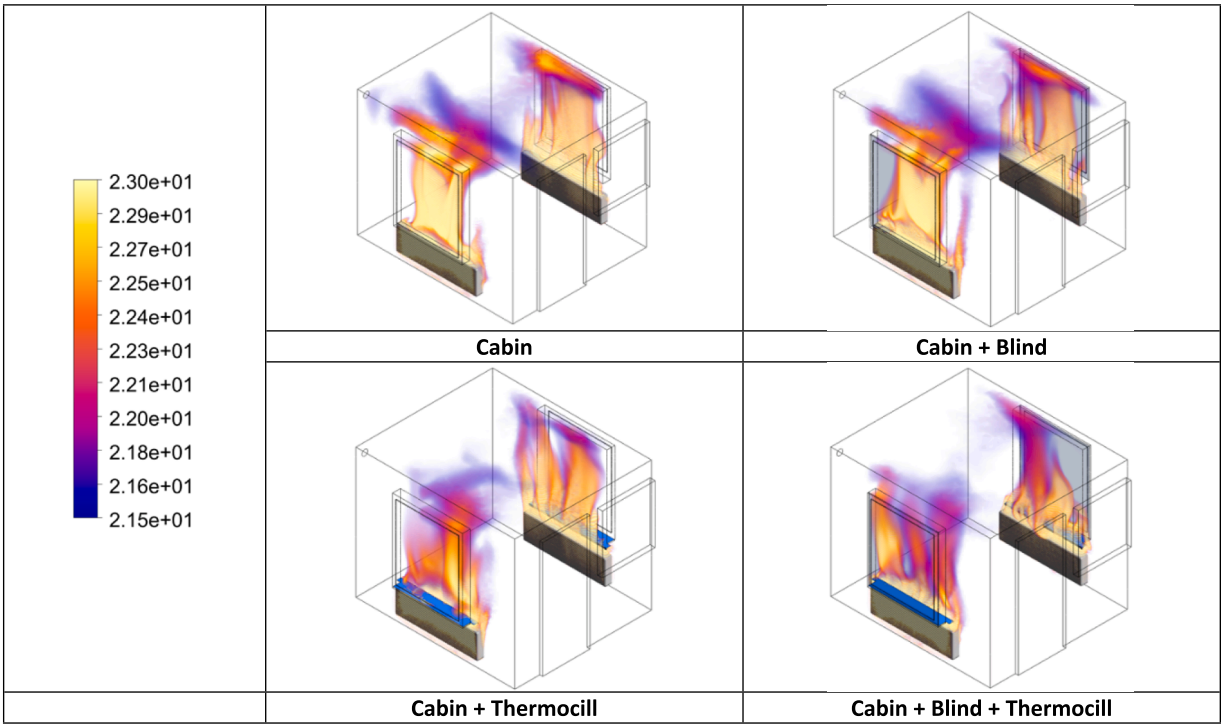

Fig. 11. Volume-rendered temperature contours for different test cases and cabin temperature setpoint of 21 °C. For each case, the temperature legend is capped between 'setpoint + 0.5 °C' and 'setpoint + 2 °C'.

Table 6
Comparing heat loss improvement by implementing blind and Thermocill (%).

Temperature (°C)	16	21	24
Cabin vs Cabin + Blind	−0.8 %	−1.2 %	−1.0 %
Cabin vs Cabin + Blind + Thermocill	−2.1 %	−2.3 %	−2.0 %
Cabin vs Cabin + Thermocill	0.0 %	−0.5 %	−0.4 %
Cabin + Blind vs Cabin + Blind + Thermocill	−1.3 %	−1.2 %	−1.0 %

at the time of running the simulations, therefore reasonable assumptions have been made.

- Given the room temperature, although the radiation does not impact significantly, changes in surface radiation properties can affect the impact of the Thermocill, which may improve its performance in some cases and show less efficiency for other conditions.

Some suggestions for future work are as follows:

- As demonstrated by Keshmiri [23], energy modelling for a specific building needs to be conducted to obtain the correct value of energy saving since simple analytical solutions (e.g. using basic heat loss

Table 7
U-value (W/m^2 K) for air-filled double-glazed window.

	Air-filled double glazing		
Temperature (°C)	16	21	24
Cabin	1.72	1.80	1.80
Cabin + Blind	1.44	1.47	1.49
Cabin + Thermocill	1.69	1.73	1.72
Cabin + Blind + Thermocill	1.38	1.44	1.46

Table 8
Comparing U-value (W/m^{2}K) improvement by implementing blind and Thermocill (%) for air-filled double-glazed window.

	Air-filled double glazing		
Temperature (°C)	16	21	24
Cabin vs Cabin + Blind	−16.3 %	−18.2 %	−16.8 %
Cabin vs Cabin + Blind + Thermocill	−19.7 %	−20.1 %	−19.0 %
Cabin vs Cabin + Thermocill	−2.0 %	−3.6 %	−4.4 %
Cabin + Blind vs Cabin + Blind + Thermocill	−4.1 %	−2.3 %	−2.6 %

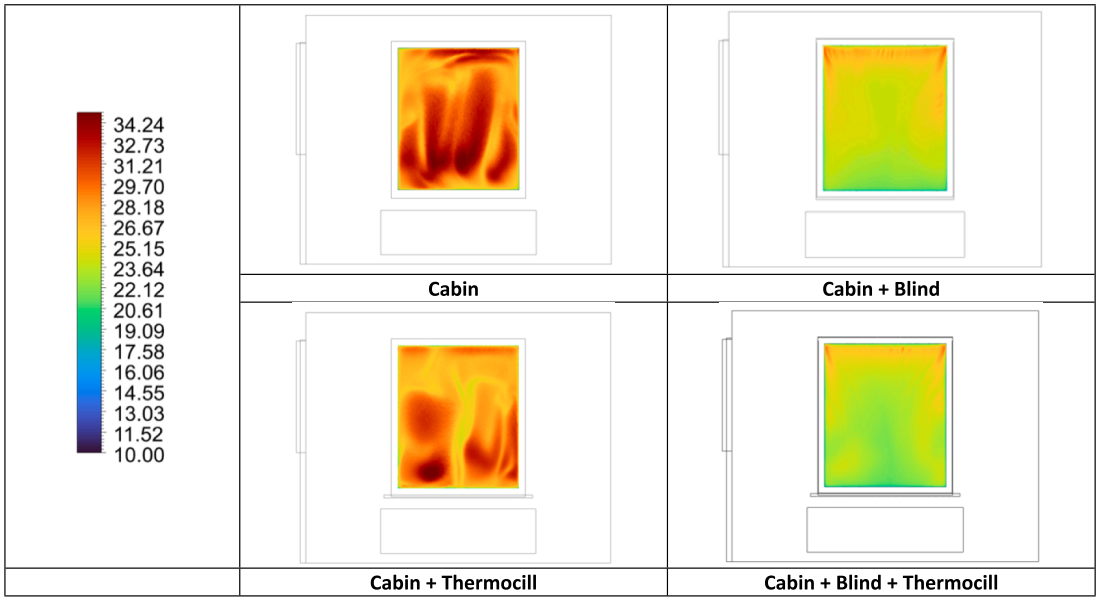

Fig. 12. Heat flux (W/m2) contours across the air-filled double-glazed window, at a temperature setpoint of 21 °C.

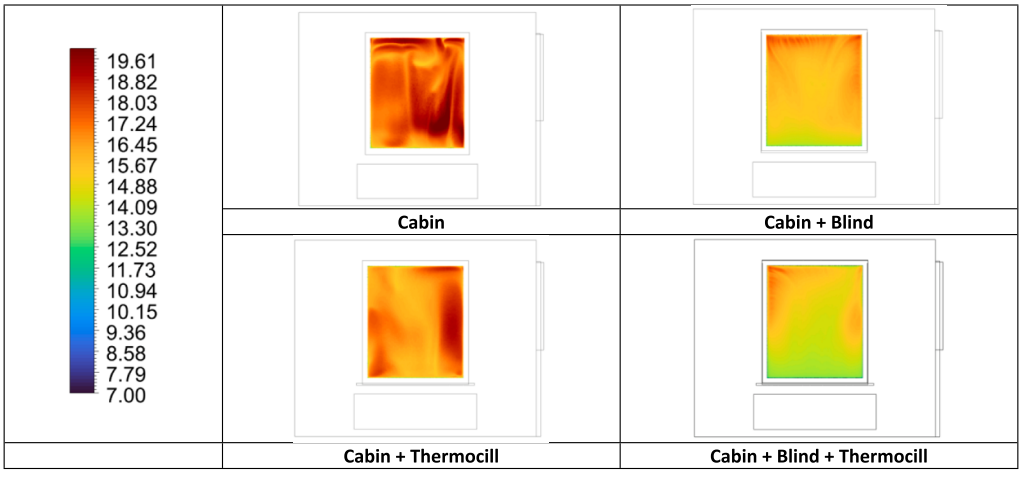

Fig. 13. Heat flux (W/m2) contours across the argon-filled double-glazed window, at a temperature setpoint of 21 °C.

Table 9
Comparing U-value (W/m^{2}K) for argon-filled double-glazed window.

Argon-filled double glazing			
Temperature (°C)	**16**	**21**	**24**
Cabin	1.06	1.06	1.05
Cabin + Blind	0.91	0.94	0.95
Cabin + Thermocill	1.01	1.02	1.04
Cabin + Blind + Thermocill	0.86	0.91	0.92

Table 10
Comparing U-value improvement by implementing blind and Thermocill (%) for argon-filled double-glazed window.

Argon-filled double glazing			
Temperature (°C)	**16**	**21**	**24**
Cabin vs Cabin + Blind	−13.3 %	−11.5 %	−8.8 %
Cabin vs Cabin + Blind + Thermocill	−18.1 %	−14.9 %	−12.3 %
Cabin vs Cabin + Thermocill	−4.2 %	−4.0 %	−1.1 %
Cabin + Blind vs Cabin + Blind + Thermocill	−5.6 %	−3.9 %	−3.8 %

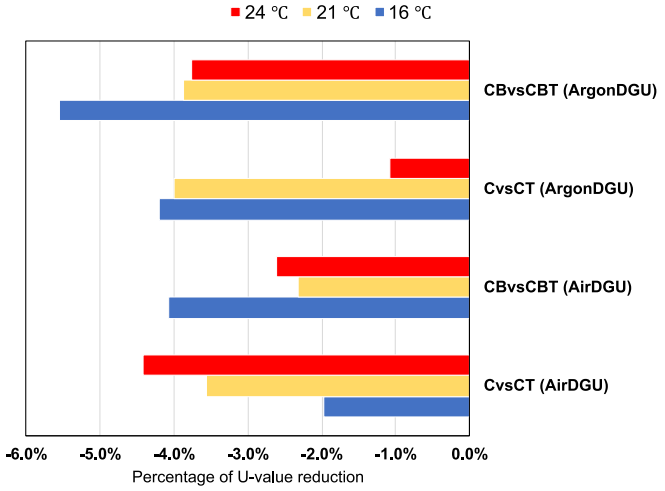

Fig. 14. Summary of the Thermocill impact on room U-value reduction. Comparisons were shown between C versus CT, and CB versus CBT for air and argon double-glazed windows; (C: Cabin, CB: Cabin and Blind, CT: Cabin and Thermocill, CBT: Cabin, Blind, and Thermocill, DG: Double-Glazed).

Table 11
Comparison of average relative reduction in U-value found experimentally and through CFD across the double-glazed window; (C: Cabin, CB: Cabin and Blind, CT: Cabin and Thermocill, CBT: Cabin, Blind, and Thermocill, DG: Double-Glazed).

Test	U-Value Reduction (%)	
	Experimental	**CFD**
C(21) vs CT(21)	2.7 % (±5.1 %)	3.6 %
CB(21) vs CBT(21)	4.0 % (±4.7 %)	2.3 %
C(24) vs CT(24)	2.7 % (±7.2 %)	4.4 %

formulas) will not provide an accurate approximation of the energy loss in a building. Therefore, one direction to continue the existing work is to conduct energy modelling for the Cabin for the same scenarios studied here, which would also represent a tool for conducting techno-economic analyses for the present problem.

- In order to obtain a more detailed picture of Thermocill performance, more cases/scenarios such as different outside temperatures, different room temperatures, various blind positions, etc are required. Once sufficient data was generated, more statistical analysis could be conducted to build more confidence in the overall performance of Thermocill and its interaction with blinds and different window types. Also, machine learning-based optimisation algorithms such as Physics-Informed Neural Networks (PINN) [36, 37] can also be used to simulate numerous scenarios in a short space of time.
- This research only considered the change in U-value, and as such the reduction in heat transfer through the window as a result of installing Thermocill. Further work should consider the hygrothermal impact the product has on the fabric of a building, particularly at junctions which are typically deemed high risk in terms of condensation and mould growth. The nature of how Thermocill works may assist with mitigating such risk, especially as this is a prominent issue observed in some fabric retrofit situations.

5. Conclusions

The impact of Thermocill on the U-value of a glazing panel has been measured through both experimental work and CFD simulation. The experimental work consisted of constructing a bespoke test cabin, within Energy House 2.0, in which Thermocill could be tested in-situ under controlled conditions, both internally and externally. In two of the three experimental tests, the average U-value of the air-filled double-glazed unit was reduced between 3–4 % when Thermocill was in operation. It was found that greater reductions in U-value were measured towards the bottom of the DGU, closer to where Thermocill is installed. This reduction was found to reduce as the distance from Thermocill (and the windowsill) increases.

The CFD work modelled the same bespoke cabin, assessing the impact of Thermocill under a greater range of conditions than what was measured experimentally. In all simulations in which Thermocill was in operation, a reduction of up to 5.6 % in the glazing U-value was observed. A good level of agreement was observed between the experimental and CFD results, owing to the close calibration of the model to the test cabin built within Energy House 2.0.

The proposed experimental and computational framework/procedure presented in this paper can be adapted and applied to other new/innovative technologies associated with building energy, helping with the implementation of new innovations under UK SAP, enabling them to be accounted for in the EPCs for Building Regulation compliance.

CRediT authorship contribution statement

Grant Henshaw: Writing – original draft, Validation, Investigation. **Amin Deyranlou:** Validation, Methodology, Investigation, Formal analysis. **Keith Rimmer:** Resources. **Heidi Paula Diaz Hernandez:** Supervision, Project administration, Methodology. **Richard Fitton:** Writing – review & editing, Supervision, Resources, Conceptualization. **Amir Keshmiri:** Writing – review & editing, Validation, Supervision, Investigation, Funding acquisition, Formal analysis, Conceptualization.

Declaration of competing interest

The authors declare the following financial interests/personal relationships which may be considered as potential competing interests: Amir Keshmiri reports financial support was provided by UK Research and Innovation. Keith Rimmer reports a relationship with Thermocill Ltd that includes: board membership and employment. Amir Keshmiri reports a relationship with Thermocill Ltd that includes: board membership. Keith Rimmer has patent UK patent (1820279.6) issued to Thermocill Ltd. Keith Rimmer is the founder and director of Thermocill Ltd and has contributed to the preparation of the paper but had no influence on the results, outcome or discussion. If there are other authors, they declare that they have no known competing financial interests or personal relationships that could have appeared to influence the work reported in this paper.

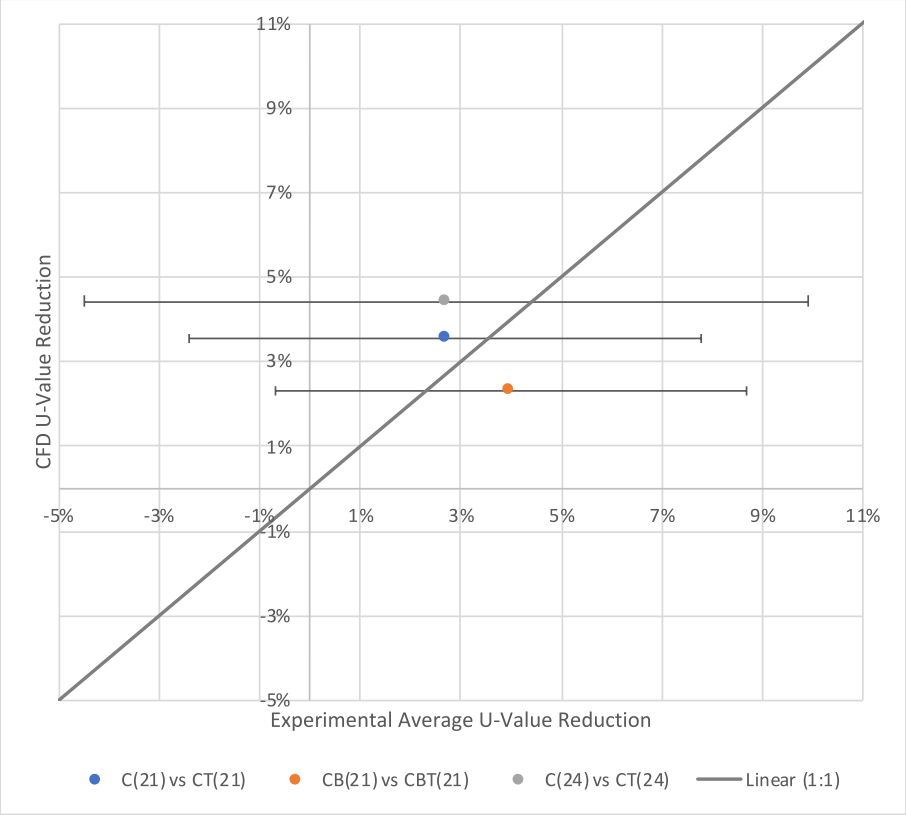

Fig. 15. Comparison between the CFD and experimental results for the 3 test scenarios on the air-filled double-glazed window; (C: Cabin, CB: Cabin and Blind, CT: Cabin and Thermocill, CBT: Cabin, Blind, and Thermocill, DG: Double-Glazed).

Data availability

Data will be made available on request.

Acknowledgements

This project was funded by the UK Engineering and Physical Sciences Research Council (EPSRC – Reference: EP/X525753/1) under the Impact Acceleration Account provided to the University of Manchester. The authors would also like to thank the team at Building Research Establishment (BRE) for providing technical input for the testing procedure presented in this work. Keith Rimmer, the CEO of Thermocill Limited would like to acknowledge the funding awarded to the company by Innovate UK and Business Growth Hub to support this project. The corresponding author would like to thank all team members of the ManchesterCFD team at the University of Manchester for their contributions to this project.

References

[1] COP26, UK Climate Leadership [WWW Document]. UN Clim. Change Conf. COP26 SEC – Glasg, 2021. URL: https://ukcop26.org/uk-presidency/uk-climate-leadership/ (accessed 7.5.22).
[2] DESNZ, UK ENERGY IN BRIEF, 2023.
[3] I. Stewart, P. Bolton, Domestic energy prices, 2023.
[4] DLUHC, The Future Homes and Buildings Standards: 2023 consultation [WWW Document], 2023. GOV.UK. URL https://www.gov.uk/government/consultations/the-future-homes-and-buildings-standards-2023-consultation/the-future-homes-and-buildings-standards-2023-consultation (accessed 12.29.23).
[5] M. Eames, M. Hunt, T. Dixon, J. Britnell, Retrofit city futures: visions for urban sustainability. Report for the Retrofit 2050, 2013.
[6] DESNZ, Net Zero Strategy, Build Back Greener, 2021.
[7] W. Swan, R. Fitton, C. Gorse, D. Farmer, M. Benjaber, The staged retrofit of a solid wall property under controlled conditions, Energy Build. 156 (2017) 250–257, https://doi.org/10.1016/j.enbuild.2017.09.033.
[8] T. Abazari, M. Mahdavinejad, Integrated model for shading and airflow window in BSk, in: Energy Procedia, CISBAT 2017 International ConferenceFuture Buildings & Districts – Energy Efficiency from Nano to Urban Scale 122, 2017, pp. 571–576, https://doi.org/10.1016/j.egypro.2017.07.423.
[9] M. Arıcı, H. Karabay, M. Kan, Flow and heat transfer in double, triple and quadruple pane windows, Energy Build. 86 (2015) 394–402, https://doi.org/10.1016/j.enbuild.2014.10.043.
[10] O. Aydın, Conjugate heat transfer analysis of double pane windows, Build. Environ. 41 (2006) 109–116, https://doi.org/10.1016/j.buildenv.2005.01.011.
[11] B.P. Jelle, A. Hynd, A. Gustavsen, D. Arasteh, H. Goudey, R. Hart, Fenestration of today and tomorrow: a state-of-the-art review and future research opportunities, Sol. Energy Mater. Sol. Cells 96 (2012) 1–28, https://doi.org/10.1016/j.solmat.2011.08.010.
[12] Z. Zhang, A. Bejan, J.L. Lage, Natural convection in a vertical enclosure with internal permeable screen, J. Heat Transf. 113 (1991) 377–383, https://doi.org/10.1115/1.2910572.
[13] T. Ariosto, A.M. Memari, K. Blansett, A. Memari, Evaluation of Residential Window Retrofit Solutions for Energy Efficiency, Pa. Hous. Res Cent, 2013.
[14] J.M. Djoković, R.R. Nikolić, O. Bokůvka, J. Pastorková, Influence of window roller blinds on energy consumption in residential buildings in Serbia, Syst. Saf. Hum. - Tech. Facil. - Environ. 5 (2023) 75–82, https://doi.org/10.2478/czoto-2023-0009.
[15] X. Fang, A study of the U-factor of a window with a cloth curtain, Appl. Therm. Eng. 21 (2001) 549–558, https://doi.org/10.1016/S1359-4311(00)00071-5.
[16] R. Garber-Slaght, C. Craven, Evaluating window insulation for cold climates, J. Green Build. 7 (2012) 32–48, https://doi.org/10.3992/jgb.7.3.32.
[17] C. Misiopecki, A. Gustavsen, B.P. Jelle, Investigating influence of different shading devices on window thermal performance, in: 13th Conference of International Building Performance Simulation Association, Chambéry, France, August 2013, 2013.
[18] D. Wang, Y. Liu, Y. Wang, Q. Zhang, J. Liu, Theoretical and experimental research on the additional thermal resistance of a built-in curtain on a glazed window, Energy Build. 88 (2015) 68–77, https://doi.org/10.1016/j.enbuild.2014.11.047.
[19] R. Fitton, W. Swan, T. Hughes, M. Benjaber, The thermal performance of window coverings in a whole house test facility with single-glazed sash windows, Energy Effic. 10 (2017) 1419–1431, https://doi.org/10.1007/s12053-017-9529-0.
[20] G. Henshaw, D. Farmer, B. George, Salford Energy House Thermal Performance of Blinds and Shutters, 2023.
[21] ISO, Thermal insulation – Building elements – In situ measurement of thermal resistance and thermal transmittance. Part 1: Heat flow meter method (No. ISO 9869-1:2014), 2014.

[22] D. Mumovic, I. Ridley, T. Oreszczyn, M. Davies, Condensation risk: comparison of steady-state and transient methods, Build. Serv. Eng. Res. Technol. 27 (2006) 219–233, https://doi.org/10.1191/0143624406bse163oa.
[23] A. Keshmiri, Drying Rate Calculations and Energy Modelling of Thermocill: A Technical Report, University of Manchester, Engineering Archive, 2020 https://doi.org/10.31224/3874.
[24] RadiWarm Signature Range, RadiWarm Pipeless Radiators, 2023. URL: https://radiwarm.com/product/radiwarm-pipeless-radiator/ (accessed 11.20.23).
[25] S. Kelly, M. Shipworth, D. Shipworth, M. Gentry, A. Wright, M. Pollitt, D. Crawford-Brown, K. Lomas, Predicting the diversity of internal temperatures from the English residential sector using panel methods, Appl. Energy 102 (2013) 601–621, https://doi.org/10.1016/j.apenergy.2012.08.015.
[26] ISO, ISO 7345: Thermal performance of buildings and building components—physical quantities and definitions, 2018.
[27] British Standards Institution, Uncertainty of measurement. Guide to the expression of uncertainty in measurement (GUM:1995). Extension to any number of output quantities (ISO 98-3:2008), 2011.
[28] A. Hosseinzadeh, A. Keshmiri, The role of turbulence models in simulating urban microclimate. Advances in heat transfer and thermal engineering, in: Proceedings of 16th UK Heat Transfer Conference (UKHTC2019), 2021, pp. 675–680.
[29] A. Hosseinzadeh, A. Keshmiri, Computational simulation of wind microclimate in complex urban models and mitigation using trees, Buildings 11 (3) (2021) 112.
[30] A. Hosseinzadeh, A. Bottacin-Busolin, A. Keshmiri, A parametric study on the effects of green roofs, green walls and trees on air quality, temperature and velocity, Buildings 12 (12) (2022) 2159.
[31] A. Keshmiri, M.A. Cotton, Y. Addad, D. Laurence, Turbulence models and large eddy simulations applied to ascending mixed convection flows, Flow Turbul. Combust. 89 (2012) 407–434, https://doi.org/10.1007/s10494-012-9401-4.
[32] A. Keshmri, J. Uribe, N. Shokri, Benchmarking of three different CFD codes in simulating natural, forced and mixed convection flows, Numer. Heat Transf. Part A Appl. 67 (2015), https://doi.org/10.1080/10407782.2014.965115.
[33] F.R. Menter, Zonal two equation k-omega turbulence models for aerodynamic flows, AIAA Paper 93–2906 (1993), https://doi.org/10.2514/6.1993-2906.
[34] HygroVUE10 – Digital Temperature and Relative Humidity Sensor with M12 Connector [WWW Document], 2024. URL: https://www.campbellsci.com/hygrovue10 (accessed 11.17.23).
[35] HFP01 heat flux plate | Hukseflux | the world's most popular heat flux sensor [WWW Document], 2023. URL: https://www.hukseflux.com/products/heat-flux-sensors/heat-flux-sensors/hfp01-heat-flux-sensor (accessed 11.17.23).
[36] Jalili, D., Jang, S., Jadidi, M., Giustini, G., Keshmiri, A., & Mahmoudi, Y., Physics-Informed Neural Networks for Heat Transfer Prediction in Two-Phase Flows, Int. J. Heat Mass Transfer, 221, 125089, 2023.
[37] Jalili, D., Jadidi, M., Keshmiri, A., Chakraborty, B., Georgoulas, A. & Mahmoudi, Y., *'Transfer learning through physics-informed neural networks for bubble growth in superheated liquid domains'*, International Journal of Heat and Mass Transfer 232, 125940, 2024.